RNA channelling by the eukaryotic exosome

Hélène Malet[1], Maya Topf[1], Daniel K. Clare[1], Judith Ebert[2], Fabien Bonneau[2], Jerome Basquin[2], Karolina Drazkowska[3,4], Rafal Tomecki[3,4], Andrzej Dziembowski[3,4], Elena Conti[2], Helen R. Saibil[1] and Esben Lorentzen[1*]

[1] Institute of Structural and Molecular Biology, Crystallography, Birkbeck College, Malet Street, London, WC1E 7HX, UK

[2] Max-Planck-Institute of Biochemistry, Department of Structural Cell Biology, Am Klopferspitz 18, D-82152 Martinsried, Germany

[3] Institute of Biochemistry and Biophysics, Polish Academy of Sciences, Pawinskiego 5a, 02-106 Warsaw, Poland

[4] Department of Genetics & Biotechnology, Faculty of Biology, University of Warsaw, Pawinskiego 5a, 02-106 Warsaw, Poland

* Corresponding author

E-mail: lorentze@biochem.mpg.de

Phone: + 49 (89) 8578 – 3479

Fax: +49 (89) 8578 – 3605

27485 characters including spaces

Running Title: Cryo-EM structures of the yeast exosome

Keywords: Exosome; RNA degradation; Cryo-EM; Macromolecular complex

Abstract

The eukaryotic exosome is a key nuclease for degradation, processing and quality control of a wide variety of RNAs. Here we report EM reconstructions and pseudo-atomic models of the 10-subunit *S. cerevisiae* exosome in the unbound and the RNA-bound states. In the RNA-bound structures, extra density visible at the entry and exit sites of the exosome channel indicates a substrate threading mechanism by the eukaryotic exosome. This channelling mechanism appears to be conserved in exosome-like complexes from all domains of life and may have been present in a last common ancestor.

Introduction

The RNA exosome is a multiprotein complex that participates in several different RNA degradation and processing reactions. Exosome function ranges from processing of stable RNAs such as ribosomal RNA (rRNA), small nuclear (snRNA) and nucleolar RNA (snoRNA), to the complete turnover of mRNA (Ibrahim et al, 2008). In addition, the exosome is involved in several surveillance pathways that target pre-mRNA with maturation defects, hypomethylated tRNA as well as incorrectly assembled pre-ribosomes (Dez et al, 2006; Hilleren et al, 2001; Kadaba et al, 2006). Consistent with its central role in RNA metabolism, the exosome is conserved in eukaryotic organisms as divergent as yeast, trypanosomes, flies, plants and humans and is also present in archaea (Lorentzen et al, 2008a; Schilders et al, 2006).

All exosomes share a common structural core of nine subunits (Exo9) as evident from crystal structures of archaeal and human exosomes (Buttner et al, 2005; Liu et al, 2006; Lorentzen et al, 2007). Six subunits (Rrp41, Rrp42, Rrp43, Rrp45, Rrp46 and Mtr3 in eukaryotes) adopt the RNase PH fold present in phosphorolytic RNases and form a hexameric ring structure surrounding a central channel (Figure 1). One side of this hexamer associates with the three additional core subunits Rrp4, Rrp40 and Csl4, which contain S1 and KH putative nucleic-acid binding domains. This structural arrangement creates a continuous channel spanning Exo9 from the S1/KH trimeric cap to the hexameric RNase PH ring. All of the exosome RNase PH subunits in both the yeast and the human complex have accumulated mutations in the phosphorolytic active sites, rendering the Exo9 complex inactive as a nuclease (Dziembowski et al, 2007; Liu et al, 2006). Instead, the RNase activity is mediated by a tenth subunit,

Rrp44, which in yeast stably associates with Exo9 to form the active ten-subunit complex (Exo10).

Rrp44 is a multi-domain protein composed of a PilT N-terminal (PIN) domain that has endonucleolytic activity followed by an RNase II/R homology region with hydrolytic exoribonuclease activity (Cheng & Deutscher, 2002; Lebreton et al, 2008; Schaeffer et al, 2009; Schneider et al, 2009). Consistent with previously published negative-stain electron microscopy (EM) data (Wang et al, 2007), a recent crystallographic structure has shown how yeast Rrp44 binds directly to the Rrp41 and Rrp45 subunits at the surface opposite the binding interface for the S1/KH subunits (Bonneau et al, 2009). These structural data are in agreement with the biochemical mapping of a 31-33 nucleotide (nt) long path suggesting that RNA substrates are threaded through the central channel of Exo9 to the Rrp44 exoribonuclease site (Bonneau et al, 2009). To further investigate this threading mechanism, we have determined EM structures of apo and RNA-bound exosome complexes from *S. cerevisiae*.

Results and Discussion

Negative-stain and cryo-EM reconstructions of the yeast exosome: organisation of the ten subunit core

The *S. cerevisiae* Exo10 complex was reconstituted from individually purified proteins and sub-complexes according to previously published protocols (Figure S1A) (Bonneau et al, 2009; Liu et al, 2006). From this sample, negative-stain and cryo-EM data were collected and 3D maps were reconstructed with resolutions of 16 Å and 14

Å, respectively (Figure S1B-C, S2A-B). Overall, the two maps display similar ring-shaped densities with a central channel characteristic of exosomes (Figure 1).

To obtain a pseudo-atomic model of the entire yeast exosome complex, crystal structures and homology models were docked into the cryo-EM map and refined using a flexible fitting method (Topf et al, 2008). Yeast Rrp40, Rrp41, Rrp45 and Rrp44 crystal structures (Bonneau et al, 2009; Lorentzen et al, 2008b; Oddone et al, 2006) and homology models of yeast Rrp4, Rrp42, Mtr3, Rrp43 and Rrp46 based on the structure of the human exosome (Liu et al, 2006) were used in the fitting procedures. For the RNase PH ring, pseudo 3-fold symmetry representing the three Rrp41/Rrp45, Rrp43/Rrp46 and Rrp42/Mtr3 dimers is clearly visible in the cryo-EM map (Figure S3A). The three cap proteins Rrp4, Rrp40 and Csl4 associate at the top of the RNase PH ring in an asymmetric manner (Figure 1). The smaller N-terminal domains of subunits Rrp40 and Csl4 had no clear density and were not included in the model. An elongated piece of density at the bottom of the RNase PH ring corresponds to the Rrp44 nuclease. Whereas the position of the PIN, exonucleolytic and S1 domains of Rrp44 are conserved compared to available crystal structures (Bonneau et al, 2009; Lorentzen et al, 2008b), CSD1 undergoes a small movement and CSD2 does not display well-ordered density suggesting that this domain is flexible in the apo Exo10 (Figure S3B). With all subunits positioned in the map, the only remaining unfilled density is located close to the PIN domain and likely corresponds to the N-terminal 36 residues not modelled in the crystal structure used for fitting (shown in a purple colour in Figure 1C). The interactions between $Rrp44_{PIN}$ and Rrp41/45 agree well with the previously published crystal structure of the Rrp44/41/45 complex (Bonneau et al, 2009). In addition, our cryo-EM map reveals that Rrp43 (residues 97-

121, 176-208 and 245-276) and $Rrp44_{CSD1}$ (residues 260-271 and 394-397) are in close proximity.

RNA protection by exosomes lacking cap subunits

Comparison of the pseudo-atomic model of the *S. cerevisiae* exosome presented here to previously published models of human and yeast exosomes (Liu et al., 2006, Wang et al., 2007) shows that the hexameric RNase PH ring is well conserved in structure with a larger degree of flexibility for the putative RNA binding subunits Csl4, Rrp4 and Rrp40 that cap the RNase PH ring (Figure S3C). The EM maps suggest smaller movements of Rrp4 but a significantly larger movement of Csl4 and Rrp40 compared to the crystal structure of the human exosome. In accordance with these observations, increased flexibility of the KH/S1 proteins has been noted in comparisons of high-resolution crystal structures of archaeal and eukaryotic exosomes (Lorentzen et al, 2007; Lu et al, 2010).

We further explored the role of the individual cap proteins in exosome assembly and RNA binding. It was previously shown that the six RNase PH subunits of the eukaryotic exosome do not form a stable complex in the absence of the three cap proteins (Liu et al, 2006). Recently, work done with truncation mutants revealed that yeast Rrp4 and Rrp40 have an important role in stabilizing the exosome structure whereas Csl4 does not (Schaeffer et al, 2009). We reconstituted and purified different exosome complexes lacking one or two cap subunits (Figure 2A). Exosomes lacking one cap subunit (Exo ΔCsl4, Exo ΔRrp4 and Exo ΔRrp40) eluted as stable complexes in size exclusion chromatography (data not shown) and were all able to bind to Rrp44 in pull-down experiments (Figure 2B). Thus, it appears that none of the cap proteins

has an essential function in forming a stable exosome. We then proceeded to test the RNA-binding abilities of Exo8 and Exo8-Rrp44 complexes in RNA protection assays similar to those recently reported for Exo10 (Bonneau et al, 2009). In this assay, a 60 nucleotides (nt) long unstructured RNA was incubated with exosome complexes and the unprotected parts of the RNA degraded with RNase A/T1. For this purpose an Rrp44(D551N) mutant that lacks catalytic activity but binds RNA was used (Lorentzen et al., 2008b). Whereas wt. Exo9 in the absence of Rrp44(D551N) does not protect RNA, Exo9 + Rrp44(D551N) protects RNA yielding fragments of 31-33 nt in length (Bonneau et al., 2009). In agreement with this, none of the reconstituted exosome complexes lacking one cap subunit was able to protect RNA in the absence of Rrp44(D551N) (lanes 2-4 in Figure 2C). With Rrp44(D551N), exosome complexes lacking one cap subunit still protect RNA (lanes 9-11 in Figure 2C). In the presence of Rrp44 (D551N), Exo ΔRrp40 behaved as Exo10, protecting 31-33 nt (Figure 2C, compare lanes 8 and 11), while Exo ΔCsl4 protected RNA fragments two nt shorter (Figure 2C, lane 9). This relatively small alteration in protection pattern may be a result of differences in RNA-binding properties of Rrp4 and Csl4 or could simply reflect that different sizes of the two cap proteins allow the RNase A/T1 to approach the RNA to a different extent. The Exo ΔRrp4 complex (Figure 2C, lane 10) displays a somewhat weaker protection pattern with a greater accumulation of degradation products, suggesting a critical role for Rrp4 in forming an exosome-RNA complex.

The finding that exosome complexes can still form and protect RNA in the absence of any one of the individual cap subunits prompted us to investigate the RNA protection patterns of exosomes lacking two cap subunits. Exosome samples containing only one cap subunit (Exo7 Csl4, Exo7 Rrp4 and Exo7 Rrp40) in the presence and absence of

Rrp44(D551N) were tested in RNA protection experiments (Figure 2C). Similarly to the wt. Exo9 complex, Exo7 complexes in the absence of Rrp44(D551N) are unable to protect RNA (Figure 2C, lanes 5-7). In the presence of Rrp44(D551N), the Csl4 containing complex only protects short 9-12 nt fragments indicating the absence of a stable exosome complex (Figure 2C, lane 12). Note that the 9-12 nt fragments correspond to the protection pattern observed for Rrp44 (D551N) alone (Bonneau et al., 2009). RNA-protection of Exo7 Rrp4 in the presence of Rrp44(D551N) also displays bands corresponding to smaller 11-12 nt fragments as well as weak bands corresponding to 21-23 nt fragments (Figure 2C, lane 13) suggesting that Rrp4 alone is not sufficient to form a fuctional exosome. In the presence of Rrp40, however, (Exo7 Rrp40 + Rrp44(D551N), Figure 2C lane 14) strong bands corresponding to fragments 27-29 nt in length are observed in addtion to the 11-12 nt fragment. This suggests that of the cap proteins, Rrp40 alone is sufficient to form a stable exosome that is functional in RNA protection *in vitro*. Judging from the increased intensity of the Rrp40 band in the Exo7 Rrp40 sample (Figure 2A, lane 7) this subunit might be present in multiple copies most likely through binding to the Rrp4 and/or Csl4 binding sites. This situation would not be unlike that for the archaeal exosome where Rrp4 and Csl4 have three identical binding sites (Buttner et al, 2005). This observed plasticity in conformation and in RNA binding by the cap proteins likely reflects the large number of different RNA substrates that are recruited and metabolised by the exosome.

EM reconstruction of substrate bound exosome: RNA is recruited via the central exosome channel

To gain direct structural insights into RNA recruitment and degradation by the eukaryotic exosome, we collected negative-stain and cryo-EM data on RNA-bound exosome samples. To verify that RNA binds under the condition of EM sample preparation, we first collected negative stain data on exosome particles bound to 5 nm gold-labelled RNA. The large gold particles allow for visualization of single RNA molecules (Figure 3A). The micrographs clearly show that every gold-labelled RNA molecule is associated with an exosome complex. Notably, the gold particles appear mostly at the center of the exosome complexes where the central channel is located.

Next, negative-stain and cryo-EM data were collected on RNA-bound exosomes and 3D maps were reconstructed at 17 Å and 12 Å resolution, respectively (Figure S2C and D). The RNA molecules have 30-40 nt long single-stranded RNA (ssRNA) extensions at the 3' end but contain bulky 5' ends that are predicted to stall at the exosome channel entrance. A pseudo-atomic model of the RNA-bound exosome was obtained for the cryo-EM map using fitting procedures as described for the apo exosome. Both the negative-stain and cryo-EM 3D reconstructions of the substrate bound exosome reveal additional density at the channel entrance compared to the reconstructions of the apo exosome (Figure 3B and C). Class averages of negative stain apo and RNA-bound exosomes also reveal this extra density (Figure S4) that likely corresponds to bound RNA as well as RNA-binding loops of Rrp4, Rrp40 and Csl4. Interestingly, the RNA density is located in close proximity to a loop of Rrp4 (residues 149-158) that contains well-conserved basic residues that could interact with RNA (R149, R150, K151) (Figure 3D). To investigate the physiological importance of these basic residues, we introduced a wild-type or a mutated (R149E, R150D and K151D) version of Rrp4 on centromeric plasmids in a yeast strain where the

chromosomal Rrp4 copy was under the control of a doxycycline-repressible promoter and tested the growth phenotypes in the presence or absence of doxycycline (Figure 3E). The mutant Rrp4 version, in contrast to the wild-type allele, did not support growth indicating that charged residues in Rrp4 loop are essential for exosome structure and/or function.

In addition to the density at the entrance channel, extra density is observed inside the central channel of the RNA-bound structures (Figure 4). The extra density is located close to secondary structure elements of Rrp41 and Rrp45 that contain well-conserved arginines ($R95_{Rrp41}$, $R96_{Rrp41}$, $R106_{Rrp45}$ and $R113_{Rrp45}$) shown to be directly involved in RNA binding by the archaeal exosome (Lorentzen & Conti, 2005). *In vitro* biochemical experiments have also shown these conserved arginines of Rrp41 to be involved in RNA binding in the yeast exosome (Bonneau et al, 2009). As the density inside the channel appears too bulky to be accounted for by ssRNA alone, it seems likely that part of the density is a result of loops of Rrp41 and Rrp45 that become ordered upon substrate binding. In particular loops 63-82, 125-138 and 167-175 of Rrp45, that interact with CSD2 domain in the crystal structure of Rrp41/44/45, are ideally positioned to account for this density. The extra density could thus, at least in part, correspond to CSD2 of Rrp44. Such a rearrangement of CSD2 upon RNA-binding in context of the Exo10 could explain previously published data showing a protection pattern of 11-12 nt for Exo10 while isolated Rrp44 gives a protection pattern of 9-12 nt (Bonneau et al, 2009).

Taken together, the data implicate an RNA threading mechanism by the eukaryotic exosome mediated by conserved sequence motifs at the entrance to and inside the

central channel (Figure 4D). The Exo9 channel could serve as a selection filter that ensures preferential degradation of RNAs with unfolded 3' ends over that of properly folded RNAs or RNAs that are bound to protein partners. Such a substrate-recruitment model provides an explanation for why the Exo9, despite being catalytically inactive, is conserved. RNA threading appears to be an evolutionarily conserved mechanism of all exosome-like complexes and might well have been present in an RNA degrading complex found in a common ancestor to all three domains of life.

Experimental procedures

Exosome sample preparation

S. cerevisiae exosome preparation, pull-down experiments and RNA protection assays were carried out as previously described (Bonneau et al, 2009; Liu et al, 2006). The 7, 8 and 9 subunit exosomes were prepared by incubating purified subunits and sub-complexes and further purified by size exclusion chromatography. In the case of Exo7 Rrp4, Exo7 Rrp40 and Exo8, peak fractions at a similar exclusion volume to that of the Exo9 were combined. For the Exo7 Csl4 complex, analysis of the peak fractions suggested that this complex is not stably associated during size exclusion chromatography. In the protection assay the exosome samples were incubated with Rrp44(D551N) in a 1.5:1 molar ratio before adding labelled RNA. For cryo-EM data collection, the *S. cerevisiae* exosome sample was diluted to a final concentration of 0.3 mg/ml and 3.5 µl applied onto glow discharged C-flat grids (CF-2/2-4C-100; Protochips). After 30s, excess solution was blotted, and the grids were flash frozen in liquid ethane. To obtain the RNA-bound complex, a concentration of 0.3 mg/ml of exosome was incubated with RNA in a 1:1.2 molar ratio (synthesized by Dharmacon,

sequence: 5'-CCCCCGAAAGGGGG$(A)_{30}$-3') for 45 min at room temperature. The complex was then vitrified as described above.

EM data collection and processing

Cryo-EM data were collected on a Polara cryo-electron microscope operated at 300 kV (FEI) using a 4k x 4k charged coupled device (CCD) camera (Gatan). Particles were manually picked in Ximdisp (Crowther et al, 1996) corrected for the effect of the contrast transfer function by phase flipping, filtered between 150 and 8 Å and normalized in SPIDER (Frank et al, 1996). Image processing and 3D reconstructions were done in SPIDER and in IMAGIC-5 (van Heel et al, 1996) and homology models were made with MODELLER-9v6 (Sali & Blundell, 1993). Fitting of atomic structures and models to the EM maps was done using UCSF Chimera (Goddard et al, 2007) and Flex-EM (Topf et al, 2008). A more comprehensive description of data processing and fitting procedures can be found in the online supplementary experimental procedures. Cryo-EM map have been deposited in EMDB with accession numbers EMD_1708 and EMD_1709 for apo and RNA-bound datasets, respectively.

Supplementary information is available at *EMBO reports* online.

References

Bonneau F, Basquin J, Ebert J, Lorentzen E, Conti E (2009) The yeast exosome functions as a macromolecular cage to channel RNA substrates for degradation. *Cell* **139**(3)**:** 547-559

Buttner K, Wenig K, Hopfner KP (2005) Structural framework for the mechanism of archaeal exosomes in RNA processing. *Mol Cell* **20**(3)**:** 461-471

Cheng ZF, Deutscher MP (2002) Purification and characterization of the Escherichia coli exoribonuclease RNase R. Comparison with RNase II. *J Biol Chem* **277**(24)**:** 21624-21629

Crowther RA, Henderson R, Smith JM (1996) MRC image processing programs. *J Struct Biol* **116**(1)**:** 9-16

Dez C, Houseley J, Tollervey D (2006) Surveillance of nuclear-restricted pre-ribosomes within a subnucleolar region of Saccharomyces cerevisiae. *EMBO J* **25**(7)**:** 1534-1546

Dziembowski A, Lorentzen E, Conti E, Seraphin B (2007) A single subunit, Dis3, is essentially responsible for yeast exosome core activity. *Nat Struct Mol Biol* **14**(1)**:** 15-22

Frank J, Radermacher M, Penczek P, Zhu J, Li Y, Ladjadj M, Leith A (1996) SPIDER and WEB: processing and visualization of images in 3D electron microscopy and related fields. *J Struct Biol* **116**(1)**:** 190-199

Goddard TD, Huang CC, Ferrin TE (2007) Visualizing density maps with UCSF Chimera. *J Struct Biol* **157**(1)**:** 281-287

Hilleren P, McCarthy T, Rosbash M, Parker R, Jensen TH (2001) Quality control of mRNA 3'-end processing is linked to the nuclear exosome. *Nature* **413**(6855)**:** 538-542

Ibrahim H, Wilusz J, Wilusz CJ (2008) RNA recognition by 3'-to-5' exonucleases: the substrate perspective. *Biochim Biophys Acta* **1779**(4)**:** 256-265

Kadaba S, Wang X, Anderson JT (2006) Nuclear RNA surveillance in Saccharomyces cerevisiae: Trf4p-dependent polyadenylation of nascent hypomethylated tRNA and an aberrant form of 5S rRNA. *RNA* **12**(3)**:** 508-521

Lebreton A, Tomecki R, Dziembowski A, Seraphin B (2008) Endonucleolytic RNA cleavage by a eukaryotic exosome. *Nature* **456**(7224)**:** 993-996

Liu Q, Greimann JC, Lima CD (2006) Reconstitution, activities, and structure of the eukaryotic RNA exosome. *Cell* **127**(6)**:** 1223-1237

Lorentzen E, Basquin J, Conti E (2008a) Structural organization of the RNA-degrading exosome. *Curr Opin Struct Biol* **18**(6)**:** 709-713

Lorentzen E, Basquin J, Tomecki R, Dziembowski A, Conti E (2008b) Structure of the active subunit of the yeast exosome core, Rrp44: diverse modes of substrate recruitment in the RNase II nuclease family. *Mol Cell* **29**(6)**:** 717-728

Lorentzen E, Conti E (2005) Structural basis of 3' end RNA recognition and exoribonucleolytic cleavage by an exosome RNase PH core. *Mol Cell* **20**(3)**:** 473-481

Lorentzen E, Dziembowski A, Lindner D, Seraphin B, Conti E (2007) RNA channelling by the archaeal exosome. *EMBO Rep* **8**(5)**:** 470-476

Lu C, Ding F, Ke A (2010) Crystal structure of the S. solfataricus archaeal exosome reveals conformational flexibility in the RNA-binding ring. *PLoS One* **5**(1)**:** e8739

Oddone A, Lorentzen E, Basquin J, Gasch A, Rybin V, Conti E, Sattler M (2006) Structural and biochemical characterization of the yeast exosome component Rrp40. *EMBO Rep* **8**(1):63-69

Sali A, Blundell TL (1993) Comparative protein modelling by satisfaction of spatial restraints. *J Mol Biol* **234**(3)**:** 779-815

Schaeffer D, Tsanova B, Barbas A, Reis FP, Dastidar EG, Sanchez-Rotunno M, Arraiano CM, van Hoof A (2009) The exosome contains domains with specific endoribonuclease, exoribonuclease and cytoplasmic mRNA decay activities. *Nat Struct Mol Biol* **16**(1)**:** 56-62

Schilders G, van Dijk E, Raijmakers R, Pruijn GJ (2006) Cell and molecular biology of the exosome: how to make or break an RNA. *Int Rev Cytol* **251:** 159-208

Schneider C, Leung E, Brown J, Tollervey D (2009) The N-terminal PIN domain of the exosome subunit Rrp44 harbors endonuclease activity and tethers Rrp44 to the yeast core exosome. *Nucleic Acids Res* **37**(4)**:** 1127-1140

Topf M, Lasker K, Webb B, Wolfson H, Chiu W, Sali A (2008) Protein structure fitting and refinement guided by cryo-EM density. *Structure* **16**(2)**:** 295-307

van Heel M, Harauz G, Orlova EV, Schmidt R, Schatz M (1996) A new generation of the IMAGIC image processing system. *J Struct Biol* **116**(1)**:** 17-24

Wang HW, Wang J, Ding F, Callahan K, Bratkowski MA, Butler JS, Nogales E, Ke A (2007) Architecture of the yeast Rrp44 exosome complex suggests routes of RNA recruitment for 3' end processing. *Proc Natl Acad Sci U S A* **104**(43)**:** 16844-16849

Acknowledgements

This work was supported by the 3D Repertoire EU grant to H.R.S., E.C. and A.D. and the EUxosome ESF grant to H.R.S. and A.D. Funding by an EMBO installation grant, Polish State grants (N N301 160335, N N301 251336) as well as a TEAM grant from the Foundation for Polish Science to A.D, by the Wellcome Trust to H.R.S and by the Max Planck Gesellschaft, the SFB646 and the Leibniz Program of the DFG to E.C. is

acknowledged. E.L. was supported by FEBS and HFSP postdoctoral fellowships. M.T. is funded by an MRC Career Development Award.

Figure legends

Figure 1) Cryo-EM structure of the *S. cerevisiae* exosome

(A) Schematic representation of the eukaryotic exosome architecture. The ribonuclease Rrp44 is positioned at the bottom of Exo9. (B) Side and top views of the apo exosome EM map as a white surface with the fitted atomic coordinates of the exosome subunits displayed as ribbons. (C) Zoom-in views of the domains of the Rrp44 subunit. The PIN, CSD1, exoribonuclease and S1 domains are shown as ribbons and the position of the N-terminal of the PIN domain is colored purple. The right hand panel shows an orthogonal slice of the EM map. Interactions of Rrp44 domains with RNase PH subunits of the exosome are indicated.

Figure 2) Role of the cap subunits in RNA recruitment

(A) SDS gel showing the reconstituted Exo9 (lane 1), Exo8 (lanes 2-4) and Exo7 (lanes 5-7) after size exclusion chromatography. (B) Purified Exo9 (lane 1) and exosome complexes containing any two of the three cap subunits (Exo ΔCsl4, Exo ΔRrp4 or Exo ΔRrp40, lanes 2-4) form stable complexes that bind Rrp44 (D551N RNase inactive mutant) in pull-down experiments (lanes 5-8). (C) RNA protection assay. The purified exosome complexes were incubated with a 60 nt long RNA molecule and unprotected RNA degraded with RNase A/T1. RNA protection by exosomes without Rrp44 is shown in lanes 1-7 and the protection by Rrp44(D551N)-containing exosomes in lanes 8-14.

Figure 3) Structural evidence of RNA binding at the channel entrance

(A) Negative stain micrograph of exosomes bound to gold-labelled RNA. The 5' biotinylated RNA is coupled to streptavidin covalently linked to 5 nm gold particles (black dots). (B) Top view of cryo maps of apo (left) and RNA-bound exosome (right) with fitted exosome subunits. Additional density located at the entrance of the central channel in the RNA-bound map is colored red. One loop of Rrp4 (shown in black) is in close proximity to this density and contains conserved residues. (C) Top view of negative stain EM maps of apo (left) and RNA-bound exosome (right) with extra density present in the RNA-bound map colored in red. (D) Sequence alignment of the Rrp4 loop in close proximity to the additional density observed in the RNA-bound exosome (loop colored black in figure 3B). *S. cerevisiae*, *S. pombe*, *H. sapiens*, *D. melanogaster, C. elegans* and *S. solfataricus* sequences are aligned. Conserved basic residues are shown in blue and conserved acidic residues are shown in red. (E) Growth phenotypes resulting from expression of plasmid-borne wt and R149E, R150D, K151D mutant Rrp4 in a yeast strain where the chromosomal Rrp4 copy is under the control of a doxycycline-repressible promoter. Alleles were assessed in the presence or absence of doxycycline (DOX) after incubation for 60h at 30 °C.

Figure 4) RNA threading through the exosome channel

(A) Side views of cryo-EM maps of apo (left) and RNA-bound exosomes (right). The extra densities at the entrance and exit of the channel are colored in red and orange respectively. Loops of Rrp45 that become visible in the EM map upon RNA binding are shown in black. (B) Side views of negative stain EM maps of apo (left) and RNA-bound exosomes (right). Extra densities present in the RNA-bound map are shown as in (A). (C) Difference maps calculated between the RNA-bound and the apo cryo-EM

maps. Positive (density appearing upon RNA binding) and negative difference maps are shown in orange and blue, respectively. (D) Slice through the RNA-bound exosome displaying the central channel of the complex. Extra densities present in the RNA-bound map are shown in red and orange. The proposed RNA recruitment path via the central channel is shown as a black line.

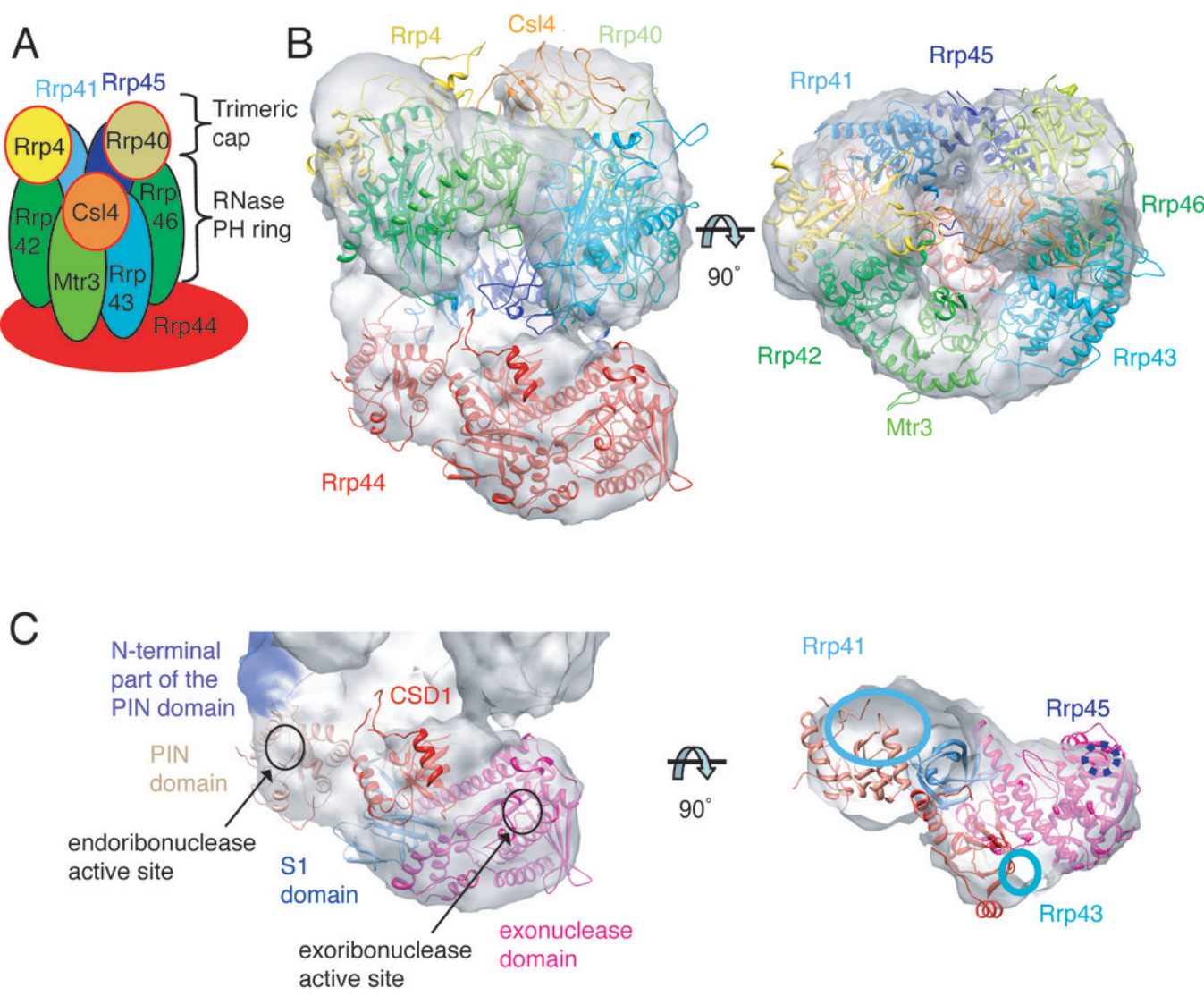
A
Rrp41
Rrp45
Rrp4
Rrp40
Csl4
Rrp 42
Rrp 46
Mtr3
Rrp 43
Rrp44
Trimeric cap
RNase PH ring
B
Rrp4
Csl4
Rrp40
Rrp44
90˚
Rrp45
Rrp41
Rrp46
Rrp42
Rrp43
Mtr3

C
N-terminal part of the PIN domain
PIN domain
endoribonuclease active site
CSD1
S1 domain
exoribonuclease active site
exonuclease domain
90˚
Rrp41
Rrp45
Rrp43

Figure 1

A

Lane number	1	2	3	4	5	6	7
Exo9 wt	+						
Exo8 ΔCsl4		+					
Exo8 ΔRrp4			+				
Exo8 ΔRrp40				+			
Exo7 Csl4					+		
Exo7 Rrp4						+	
Exo7 Rrp40							+

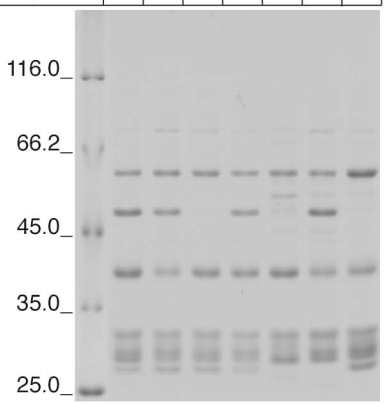

B

Lane number	1	2	3	4	5	6	7	8
Rrp44 D551N					+	+	+	+
Exo9 wt	+				+			
Exo8 ΔCsl4		+				+		
Exo8 ΔRrp4			+				+	
Exo8 ΔRrp40				+				+

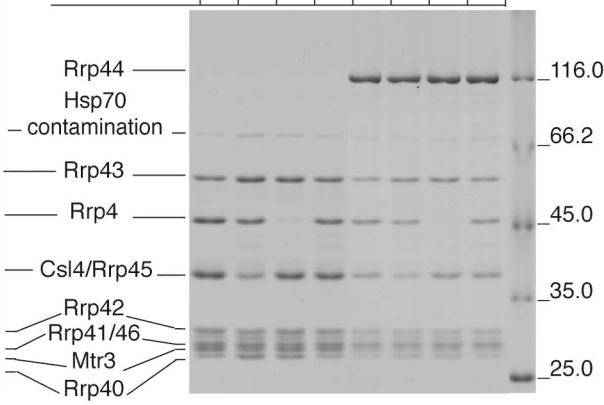

C

Lane number	1	2	3	4	5	6	7	8	9	10	11	12	13	14	15	16
Rrp44 D551N								+	+	+	+	+	+	+		
Exo9 wt	+							+								
Exo8 ΔCsl4		+							+							
Exo8 ΔRrp4			+							+						
Exo8 ΔRrp40				+							+					
Exo7 Csl4					+							+				
Exo7 Rrp4						+							+			
Exo7 Rrp40							+							+		
60-mer RNA	+	+	+	+	+	+	+	+	+	+	+	+	+	+	+	+
RNase A/T1	+	+	+	+	+	+	+	+	+	+	+	+	+	+	+	

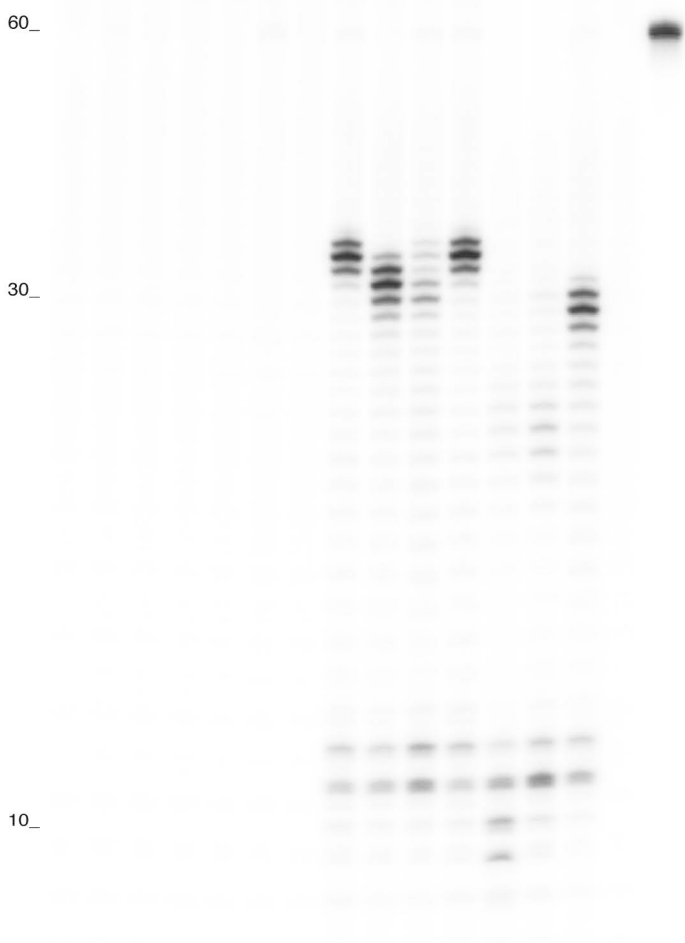

Figure 2

A

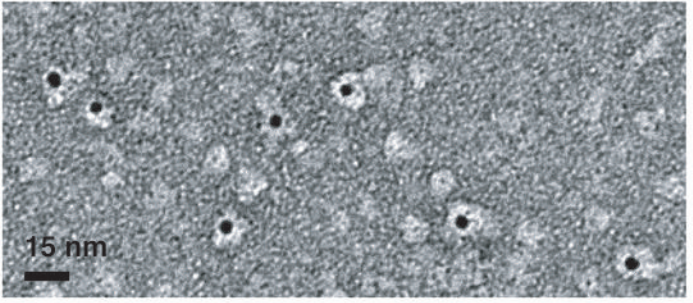

Negative stain RNA-bound exosome labeled at the RNA 5' end with a 5 nm gold particle

B

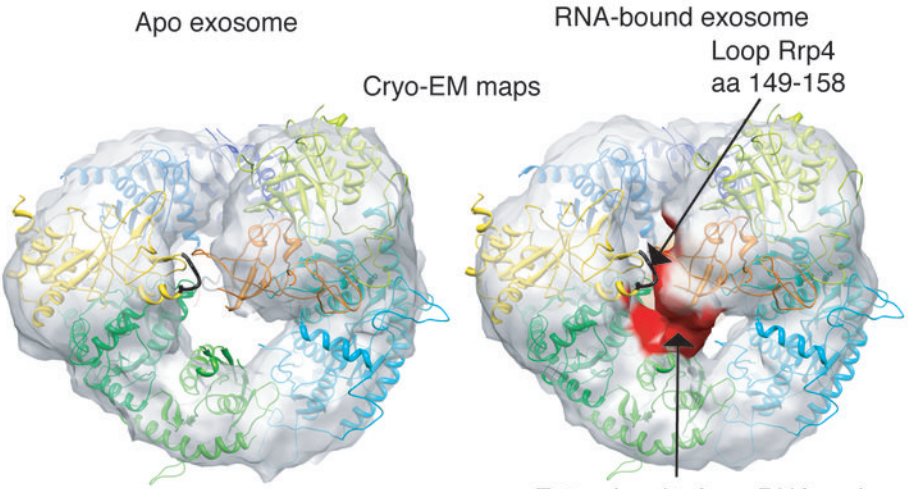

C

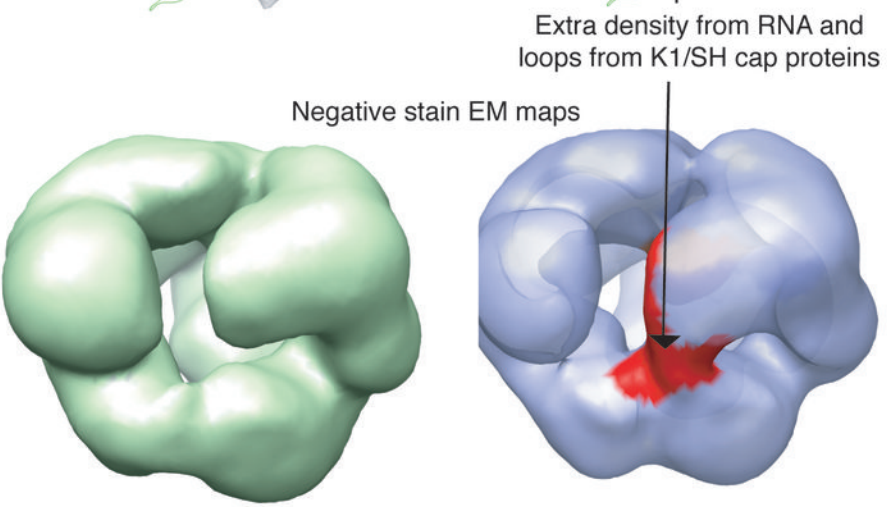

D

α1

S.cerevisiae	Rrp4	144	PGGILRRKSESDELQ	158
S.pombe	Rrp4	147	PGGIQRRKLETDELQ	161
H.sapiens	Rrp4	116	PGGELRRRSAEDELA	130
D.melanogaster	Rrp4	119	PGGELRRRSAEDEQM	133
C.elegans	Rrp4	122	PGGDFRRKDVEDEEK	136
S.sulfataricus	Rrp4	103	PASNLLGRSINVGED	117

E

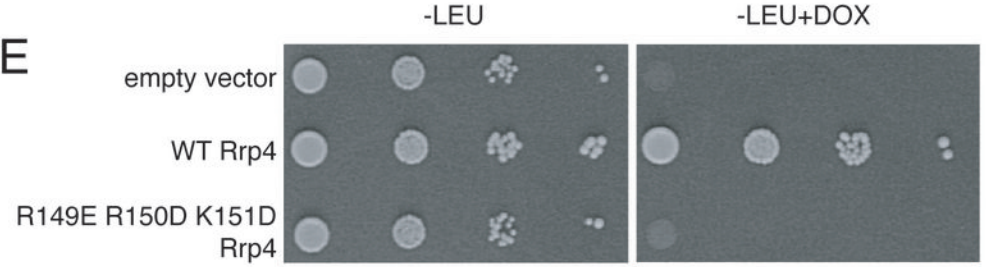

Figure 3

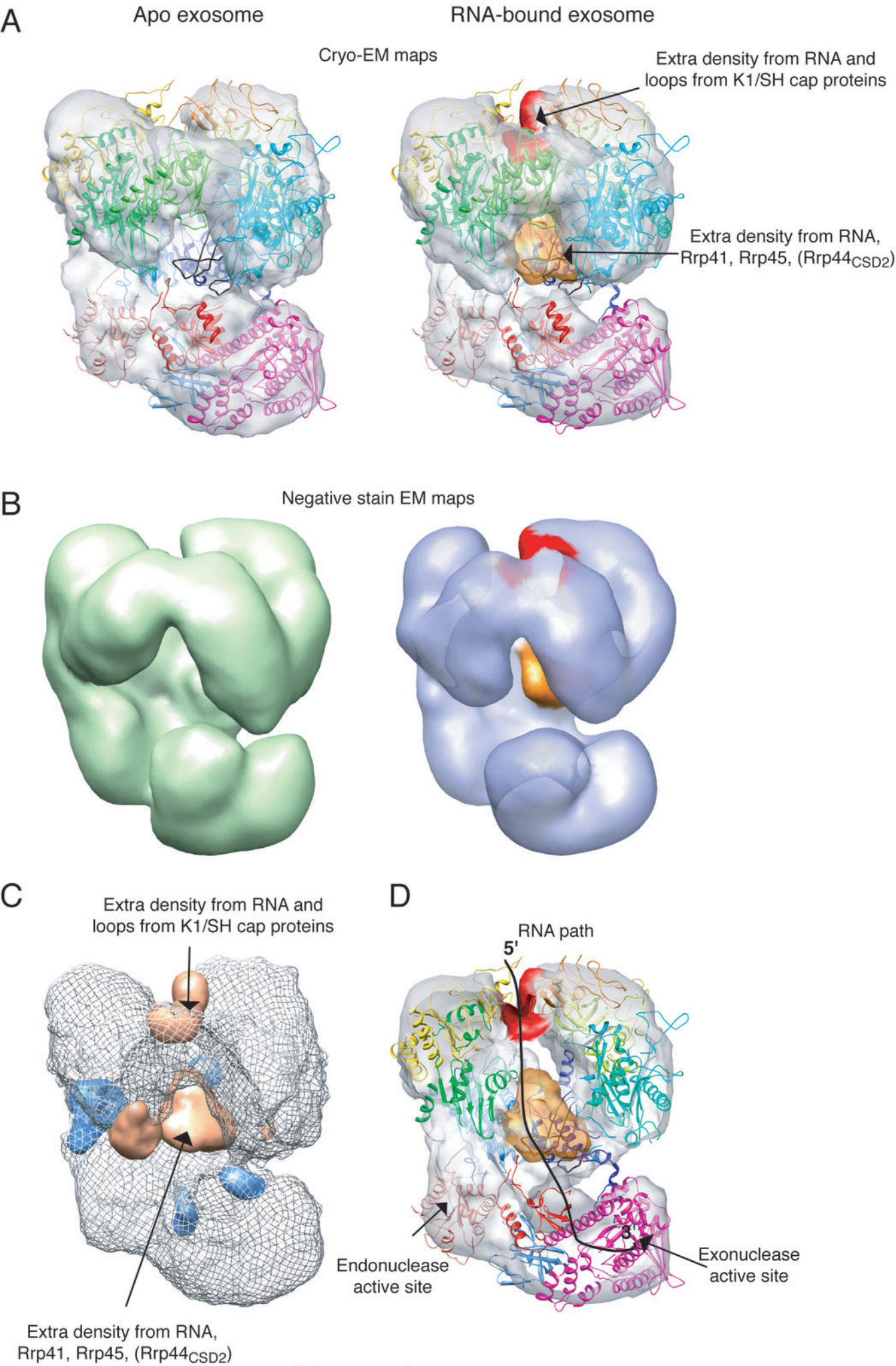
A
Apo exosome
RNA-bound exosome
Cryo-EM maps
Extra density from RNA and loops from K1/SH cap proteins
Extra density from RNA, Rrp41, Rrp45, (Rrp44CSD2)
B
Negative stain EM maps
C
Extra density from RNA and loops from K1/SH cap proteins
Extra density from RNA, Rrp41, Rrp45, (Rrp44CSD2)
D
RNA path
5'
3'
Endonuclease active site
Exonuclease active site

Figure 4